Metastable Metals

DOI: 10.1002/anie.201101248

A Metastable Metal with Decagonal Local Symmetry Obtained by Low-Temperature Pseudomorphosis

*Martin Kaiser, Anna Isaeva, and Michael Ruck**

Metastable metallic phases are hard to isolate owing to the lack of directed covalent interactions, which would hinder further phase transitions into thermodynamically stable states. The conventional approach, a very rapid quenching of melts, usually produces metallic glasses instead of quasi-crystalline or periodic structures.[1] We have now succeeded in the synthesis of a metastable intermetallic compound with complex crystalline order by the low-temperature transformation of a solid precursor.

$Bi_{28}Ni_{25}$ (**1**) was obtained by reduction of the subiodide $Bi_{28}Ni_{25}I_5$[2] with *n*BuLi at 69 °C (the boiling point of *n*-hexane) within two days. In a pseudomorphosis, the iodine component was completely extracted while the needle-shaped crystals were preserved (Figure 1).

X-ray diffraction on a single-crystal revealed that the intermetallic fragments of the precursor survived the procedure and rearranged themselves into a unique crystal structure (Figure 2). These fragments are decagonal rods of about 1 nm in diameter, which consist of an outer bismuth tube and an inner nickel tube. The rhombus motif of the outer Bi net clearly differs from the chair-conformation rings in double-walled Bi nanotubes.[3] As in $Bi_{28}Ni_{25}I_5$, the Bi–Ni rods contain additional Bi_{axis} atoms on the central axis, which have different periodicity to the rest of the structure: There are 6 Bi_{axis} atoms per 5 lattice translations along *b*. Occupancies and interatomic distances suggest an ordered sequence within a rod, which, however, is not coherent between neighboring nanorods (no superstructure reflections).

The reduction causes a shrinkage of the unit cell along *c* ($\Delta a/a = +4\,\%$, $\Delta b/b = +0.8\,\%$, $\Delta c/c = -16\,\%$) and a volume decrease of about 30 Å^3 per iodide ion, which corresponds well with the volume increment given by Biltz.[4] The shifting of the Bi–Ni rods towards each other is accompanied by a small rotation of only 4.5°. Thereby many new inter-rod

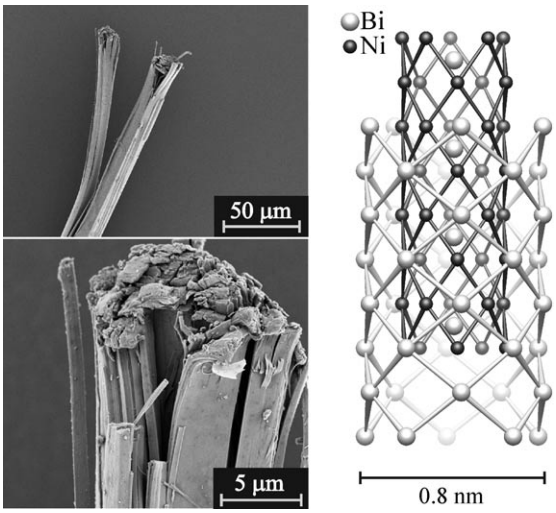

Figure 1. Left: SEM micrographs of **1** after pseudomorphosis of $Bi_{28}Ni_{25}I_5$, and right: characteristic decagonal nanorod of coaxial Bi and Ni tubes.

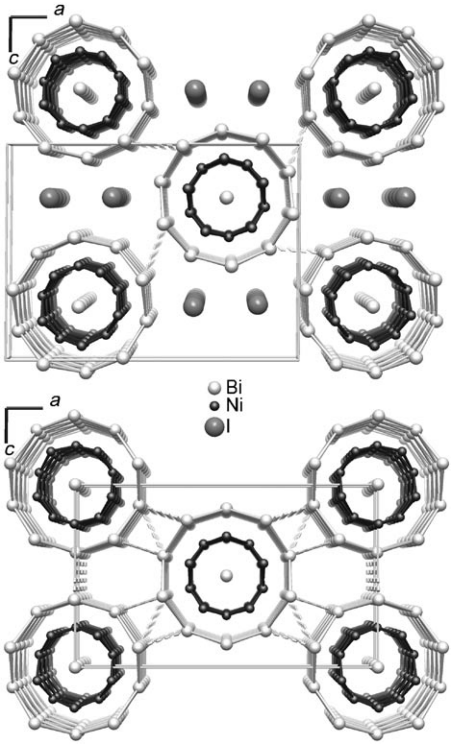

Figure 2. The structures of top: the monoclinic subiodide $Bi_{28}Ni_{25}I_5$ and bottom: the orthorhombic intermetallic $Bi_{28}Ni_{25}$ drawn on the same scale. Lines that represent the Bi–Ni bonding are omitted for clarity.

[*] M. Kaiser, Dr. A. Isaeva, Prof. Dr. M. Ruck
Department of Chemistry and Food Chemistry
Dresden University of Technology
01062 Dresden (Germany)
Fax: (+49) 351-463-37287
E-mail: michael.ruck@tu-dresden.de
Prof. Dr. M. Ruck
Max Planck Institute for Chemical Physics of Solids
Nöthnitzer Strasse 40, 01187 Dresden (Germany)

Supporting information for this article is available on the WWW under http://dx.doi.org/10.1002/anie.201101248.

contacts are established [d(Bi–Bi) $\geq$ 3.59 Å] and the circular cross-section of the rod is slightly deformed to an elliptical one. A detailed synopsis of structural characteristics of the two compounds is given in the Supporting Information (Table S2).

Little is known about the mechanism of the heterogeneous reaction that drives the transformation. The formation of a new and dense packing of the intermetallic rods and the split ends of the needles suggest that the iodide ions leave the crystal along the channels in b direction. Moreover, the dislocations and cracks that result from the shrinking (Figure 1) open further diffusion paths. Possibly the injection of electrons by nBu groups that coordinate to the outer surface pushes out the iodide ions, which are then trapped as a LiI precipitate.

Compound **1** decomposes exothermically into BiNi (NiAs type)[5] and some Bi_3Ni[6] upon heating to about 145(5) °C (Supporting Information; Figure S1). Thus, **1** is metastable (probably under all conditions) and not part of the binary phase diagram.

Electrical measurements on a single-crystal of **1** revealed good metallic conductivity along the needle axis, that is, the b direction [$\rho(300\,\mathrm{K}) = 7.1 \times 10^{-6}\,\Omega\,\mathrm{m}$]. Characteristic for a highly defective conductor, the temperature gradient is only $10^{-8}\,\Omega\,\mathrm{m\,K^{-1}}$ (Supporting Information, Figure S2). The electronic band structure of **1** (Supporting Information, Figure S3) shows numerous bands with strong dispersion, which cross the Fermi level, corresponding to a metal without preferred direction for conduction. The intensive interaction is, however, primarily within a single rod, while transport between the weakly interacting intermetallic rods (see below) should be poor.

The bands close to the Fermi level are formed mainly by the Bi-6p and Ni-3d states, with the Ni-3d state being almost filled (Supporting Information, Figure S4). Experimentally, **1** shows Pauli paramagnetism overlaid by large diamagnetic contributions (Supporting Information, Figure S5). The bands are hardly affected by the occupancy and the position of Bi_{axis} sites, which was tested by calculations of models with varying populations of those sites (0 to 100 %). In comparison with the electronic structure of $Bi_{28}Ni_{25}I_5$, the Fermi level is elevated by approximately 0.9 eV after the reduction, however, the band distribution is nearly unchanged.

The reduction of $Bi_{28}Ni_{25}I_5$ to $Bi_{28}Ni_{25}$ adds electrons to the bonding system of the intermetallic rods. The impact was evaluated by COHP (crystal orbital Hamilton population[7]) analysis of inter-rod and intra-rod interactions (Figure 3, and Supporting Information, Figure S6). The extra electrons fill vacant bonding states in the tubes, which explains the shortening of the Bi_{outer}–Ni bonds in particular (Supporting Information, Table S2). Only a marginal increase in the population of bonding states is observed for intra-rod as well as inter-rod Bi–Bi interactions. On the other hand, the Bi_{axis}–Bi_{axis} antibonding states are filled causing an unfavorable electronic situation, which is reflected by longer interatomic distances. Yet in the ternary subiodide, the Fermi level exactly separates the bonding and antibonding states of Bi_{axis}—Bi_{axis}, that is, the charged $[Bi_{28}Ni_{25}]^{5+}$ rod seems to have the optimal electron count.

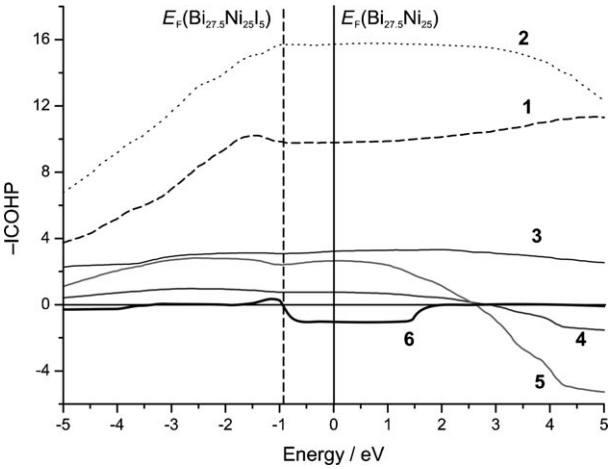

Figure 3. ICOHP (integrated COHP) calculated for $Bi_{27.5}Ni_{25}$. The Fermi-level (E_F) shift for $Bi_{27.5}Ni_{25}I_5$ is indicated by the vertical dashed line (ICOHP curves are almost identical in both compounds). 1) Ni–Ni, 2) Bi_{outer}–Ni, 3) Ni–Bi_{axis}, 4) Bi_{outer}–Bi_{axis}, 5) Bi–Bi in outer tube, 6) Bi_{axis}–Bi_{axis}.

The bonding scenario in $Bi_{28}Ni_{25}$ and $Bi_{28}Ni_{25}I_5$ was also investigated by means of topological analysis of the electron density (quantum theory of atoms in molecules, QTAIM[8]) and the electron localizability indicator (ELI-D, Y^{σ}_{D}).[9] Bader charges are listed in Supporting Information, Table S3. ELI-D is a 3D real-space indicator, which classifies certain regions of space as atomic cores, lone pairs, or chemical bonds. The absence of any attractor confirms the purely electrostatic nature of I^- and $[Bi_{28}Ni_{25}]^{5+}$ interactions in the subiodide. In both compounds, strong pair-wise Ni–Ni bonding (ca. 2.5 electrons) is found in the inner tube (Supporting Information, Figure S7a), in which the Ni atoms are in square-planar coordination environments. The region inside the nickel tube is electron poor and features only delocalized Ni–Bi_{axis} (ca. 0.4–0.6 electrons), as well as stronger Bi_{axis}–Bi_{axis} interactions (toroidal basin populated by 0.2 electrons, Figure S7b of the Supporting Information). The inter-tube Bi + 4 Ni and Bi + 2 Ni multicenter interactions are indicated by polysynaptic ELI-D basins that have 0.7 to 1.7 electrons (Supporting Information, Figure S7c, d). Hence, the inner rod of Bi_{axis} atoms is only loosely attached to the tubes, similar to the composite structure of the high-pressure allotrope bismuth-III.[10] The ELI-D shows no attractors that correspond to significant inter-rod Bi–Bi interactions. This situation may be attributed to both, the weakness of the bonds and to the applied computational methods.

In summary, the intermetallic bonding system acts as a structurally rigid electron reservoir that tolerates changes in the electron count, and thereby allows the reductive pseudomorphosis.

Experimental Section

Synthesis: $Bi_{28}Ni_{25}I_5$ was synthesized as described in literature.[2] Black crystals of **1** were obtained in 90 % yield by treating $Bi_{28}Ni_{25}I_5$ crystals (1 g, 0.13 mmol) in a freshly prepared solution of nBuLi (Sigma Aldrich; 40 equivalents with respect to $Bi_{28}Ni_{25}I_5$) in boiling

hexane (69 °C) under argon atmosphere for two days. The liquid phase was drawn off by a syringe and the solid was washed several times with hexane and ethanol. The compound is stable in air and inert to water and alcohols. The thermal decomposition under equilibrium pressure was examined using a DTA-DSC Labsys TMA System (Setaram). Chemical analysis by ICP-OES, ICP-MS, and ion chromatography (atom %) calcd: Bi 52.8, Ni 47.2: found Bi 52.5(2), Ni 46.9(2), I 0.6(1).

X-ray crystallography: Apex-II kappa CCD diffractometer (Bruker); $Mo_{K\alpha}$ radiation, $\lambda = 0.71073$ Å, $T = 293(2)$ K; numerical absorption correction;[11] structure solution with direct methods; refinements[12] against F_o^2. The refined structure model (Supporting Information, Table S1) also matches the measured powder diffraction pattern (Supporting Information, Figure S9). Graphics were generated with Diamond.[13] **1**: $Bi_{28}Ni_{25}$, *Imma* (no. 74), $a = 19.24(1)$, $b = 4.219(2)$, $c = 11.656(5)$ Å, $V = 946.2(8)$ Å^3; $Z = 0.8$; $\rho_{calcd} = 10.28$ g cm^{-3}; $\mu(Mo_{K\alpha}) = 113.4$ mm^{-1}; $2\theta_{max} = 54.4°$; 1367 measured, 605 unique reflections, $R_{int} = 0.040$, $R_o = 0.074$; 37 parameters; R_1-$[422F_o > 4\sigma(F_o)] = 0.044$, wR_2(all F_o^2) = 0.058, GooF = 1.15; residual electron density: −3.2 to 2.8 e Å^{-3}. Further details on the crystal structure investigations may be obtained from the Fachinformationszentrum Karlsruhe, 76344 Eggenstein-Leopoldshafen, Germany (fax: (+49) 7247-808-666; e-mail: crysdata@fiz-karlsruhe.de), on quoting the depository number CSD-422684.

Quantum chemical calculations: Solid-state scalar-relativistic density functional theory (DFT) calculations were performed with the TB-LMTO-ASA program[14] for $Bi_{28}Ni_{25}I_5$ and **1**, employing approximants for zero-occupancy of Bi_{axis} sites [$Bi_{25}Ni_{25}I_5$ (*I2m*) and $Bi_{25}Ni_{25}$ (*Imma*)], for 50 % occupancy of Bi_{axis} sites [$Bi_{27.5}Ni_{25}I_5$ (*P2/n*; 2b and 2d sites), and $Bi_{27.5}Ni_{25}$ (*Pmna*; *2a and 2d* sites)], and for $Bi_{30}Ni_{25}$ (*Imma*). COHP were calculated using the subroutine implemented in the TB-LMTO-ASA package.[15] Band structures and density of states plots were visualized by means of the Gnuplot program package.[16]

Chemical bonding in the compounds was characterized through the topological analysis of the electron density (ρ) and of the electron localizability indicator (ELI-D, Y).[9] Both quantities have been calculated using the ELI module implemented within the TB-LMTO-ASA program package. Atomic charge populations were computed with consecutive integration of the electron density in basins according to QTAIM.[8] Numerical analysis of ELI-D topology was performed in the DGrid 4.6[17] program by a similar procedure. The results of topological analysis were visualized using Paraview program package[18].

Received: February 18, 2011
Published online: May 17, 2011

Keywords: bismuth · intermetallic phases · metastable compounds · nickel · pseudomorphosis

[1] a) A. L. Greer, *Mater. Today* **2009**, *12*, 14–22; b) W. Steurer, S. Deloudi, *Acta Crystallogr. Sect. A* **2008**, *64*, 1–11.
[2] M. Ruck, *Z. Anorg. Allg. Chem.* **1995**, *621*, 2034–2042.
[3] a) R. Boldt, M. Kaiser, D. Köhler, F. Krumeich, M. Ruck, *Nano Lett.* **2010**, *10*, 208–210; b) B. Rasche, G. Seifert, A. Enyashin, *J. Phys. Chem. C* **2010**, *114*, 22092–22097.
[4] W. Biltz, *Raumchemie der festen Stoffe*, Verlag Leopold Voss, Leipzig **1934**.
[5] M. Ruck, *Z. Anorg. Allg. Chem.* **1999**, *625*, 2050–2054.
[6] M. Ruck, T. Söhnel, *Z. Naturforsch. B* **2006**, *61*, 785–791.
[7] R. Dronskowski, P. E. Blöchl, *J. Phys. Chem.* **1993**, *97*, 8617–8624.
[8] R. F. W. Bader, *Atoms in Molecules*, Oxford University Press, Oxford, **1990**.
[9] a) M. Kohout, *Faraday Discuss.* **2007**, *135*, 43–54; b) M. Kohout, *Int. J. Quantum Chem.* **2004**, *97*, 651–658.
[10] O. Degtyareva, M. I. McMahon, R. J. Nelmes, *Mater. Sci. Forum* **2001**, *378–381*, 469–475.
[11] SADABS-2008/1, Bruker AXS Inc., Madison (WI, USA).
[12] G. M. Sheldrick, *Acta. Crystallogr. Sect. A* **2008**, *64*, 112–122.
[13] K. Brandenburg, *Diamond 3.2g*, Crystal Impact GbR, Bonn, **2011**.
[14] O. Jepsen, A. Burkhardt, O. K. Andersen, *The Program TB-LMTO-ASA*, Version 4.7, Max Planck Institute for Solid State Research, Stuttgart, Germany, **1999**.
[15] F. Boucher, O. Jepsen, O. K. Andersen, *The Supplement to the TB-LMTO-ASA*, Version 4.7c, **1997**.
[16] T. Williams, C. Kelley, *Gnuplot 4.4: an interactive plotting program*, **2010**. http://gnuplot.sourceforge.net/.
[17] M. Kohout, *DGrid 4.6*, Radebeul, Germany, **2009**.
[18] Sandia National Labs, Kitware Inc, Los Alamos National Labs, *Paraview: Parallel visualization application*. http://paraview.org, **2008**.

